*Journal of The Electrochemical Society*, **151** (1) B22-B26 (2004)
0013-4651/2003/151(1)/B22/5/$7.00 © The Electrochemical Society, Inc.

# Positron Annihilation Spectroscopy Study of Interfacial Defects Formed by Anodic Oxidation of Aluminum

**K. R. Hebert,[a,*,z] T. Gessmann,[b,d] K. G. Lynn,[b] and P. Asoka-Kumar[c]**

[a]*Department of Chemical Engineering, Iowa State University, Ames, Iowa 50011, USA*
[b]*Department of Physics, Washington State University, Pullman, Washington 99164, USA*
[c]*Department of Physics, Lawrence Livermore National Laboratory, Livermore, California 94550, USA*

Positron annihilation spectroscopy (PAS) measurements were carried out to characterize open-volume defects associated with anodic oxidation of aluminum. The annihilation fractions with low and high momentum electrons (*S* and *W* spectral lineshape parameters, respectively) of the annihilation photopeak were determined, as a function of the positron beam energy. A subsurface defect layer, containing nanometer-scale voids in the metal near the metal/oxide film interface, was found after oxide growth, and was shown to contain new voids created by anodizing. Such interfacial voids in the metal are of interest because of their possible role as corrosion initiation sites. The *S* parameter characterizing the defect-containing layer ($S_d$) was obtained by simulation of the *S*-energy profiles. On samples with two different surface conditions, $S_d$ remained constant at its initial value during anodizing. Because $S_d$ is related to the void volume fraction in the interfacial metallic layer containing the voids, that result suggests that formation of metallic voids, and their subsequent incorporation into the growing oxide layer, occurred repeatedly at specific favored sites.
 [DOI: 10.1149/1.1631821] 

Manuscript submitted March 28, 2003; revised manuscript received July 20, 2003. Available electronically December 9, 2003.

Identification of the sites on metal surfaces where pits form during corrosion or etching would lead to enhanced control over these processes. On pure metals, such defects as dislocations, microsegregated impurities, and flaws in the surface oxide film, have been suggested as pit precursor sites, although in general, conclusive supporting evidence has not been obtained.[1] Positron-based techniques are sensitive to atomic-scale open-volume defects in solids,[2-4] and have been applied to defects at interfaces in electronic materials.[5] The present authors have explored the use of positron annihilation measurements to characterize corrosion-related defects in aluminum foils. Doppler-broadening positron annihilation spectroscopy (PAS) revealed nanometer-scale voids in the aluminum metal, within tens of nanometers of the oxide film/metal interface.[6-8] These voids were shown to be created by dissolution treatments which are also used to enhance the number of pits formed by etching aluminum for capacitor applications. The measurements indicated that the metallic surface of the voids is free of oxide, and hence would be highly reactive if exposed during uniform corrosion. Atomic force microscopy (AFM) was used to demonstrate a correspondence between interfacial voids and corrosion pits formed upon anodic etching in 1 M HCl. It was therefore hypothesized that interfacial voids serve as sites for initiation of etching or corrosion pits on aluminum.

If in fact interfacial voids in the aluminum metal act as corrosion initiation sites, fundamental understanding of void formation may lead to strategies for control of corrosion or etching processes. A possible mechanism of void formation is agglomeration of metal vacancies injected into the metal when aluminum atoms are oxidized. Previous work has established that voids are created by a variety of dissolution processes, during which such oxidation occurs continuously, and is followed by ejection of metal ions from the oxide film into solution.[6-8] Voids are also present in as-annealed samples, in which they may result from high temperature oxidation during annealing. Vacancy injection by high temperature corrosion has been established, at least in studies of alloys.[9,10] Because oxidation occurs uniformly, this mechanism may suggest that voids should form at random locations along the surface. On the other hand, other mechanisms may be possible in which the local composition or topography play a role in void formation. Mechanisms incorporating roles for surface impurities would be consistent with the important effect of impurities on the number and distribution of pits resulting from anodic etching.[11]

The possibilities of random *vs.* surface defect-mediated void formation cannot be readily distinguished in studies of dissolution treatments. The nature and distribution of any surface defects would be expected to be determined by the sample surface condition; however, substantial changes of both surface composition and topography accompany dissolution. The composition changes are due to the accumulation of noble impurities at the metal/oxide interface as the aluminum atoms are dissolved.[12,13] In the present study, the formation of interfacial voids during anodic oxidation of aluminum was investigated. During anodizing, the extent of metal consumption during film growth was controlled, and could be kept very small compared to that experienced in typical dissolution processes. In this case, changes of surface composition and topography accompanying anodic oxidation would not be significant. PAS results after anodic oxidation were obtained for two samples with different surface conditions: as-annealed and caustic-treated. These samples had distinctly different interfacial void distributions prior to oxidation.[7] The goal was to explore how the surface condition influences formation of voids.

## Experimental

The aluminum foils used in this work were manufactured for use in aluminum electrolytic capacitors (Toyo). The foils were 100 μm thick with a typical grain size of 100 μm, and their nominal purity was 99.98%. The large grain size is due to extensive annealing after rolling, *e.g.*, for 5-6 h at 600°C.[14] Impurities include Cr, Cu, Fe, Ga, Mg, Si, and Zn with bulk concentrations of order 10 wt ppm.[12]

PAS measurements were carried out on two types of anodized samples: as-received aluminum foil, and foil treated in NaOH. Caustic treatment was carried out by immersion of foils in aqueous 1 N NaOH solution for 15 min at room temperature, after which they were washed thoroughly with deionized (DI) water. Anodic oxidation of the pretreated samples was carried out in a borate buffer solution (pH 8.5-8.7) at room temperature, at a constant applied current density of 2.5 mA/cm$^2$. The current source was a potentiostat/galvanostat (EG&G PAR-273), and the counter electrode was a Pt wire. Anodic oxidation continued until attaining voltages of 27, 53, 80, and 106 V, as measured between the Al sample and the counter electrode. After anodizing, the samples were rinsed thoroughly with DI water. Chemical stripping of the anodic oxide film was accomplished by immersion for 1 min in an aqueous solution of 2% $CrO_3$ and 5% $H_3PO_4$ at 85°C.

* Electrochemical Society Active Member.
[d] Present address: Department of Electrical, Computer and Systems Engineering, Rensselaer Polytechnic Institute, Troy, NY 12180.
[z] E-mail: krhebert@iastate.edu

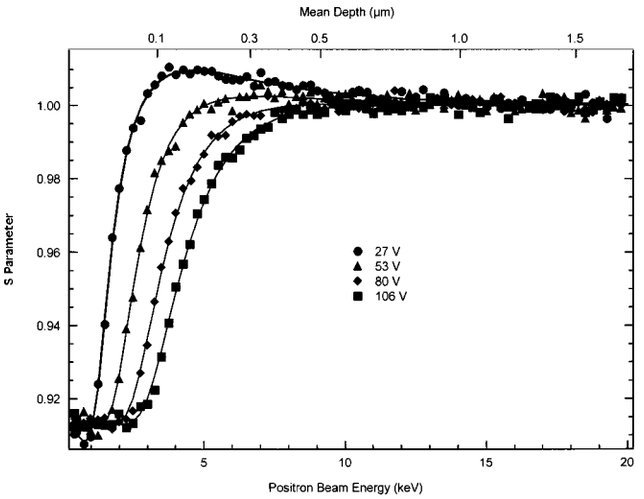


**Figure 1.** *S*-energy profiles of as-received aluminum foils after anodic oxidation at 2.5 mA/cm$^2$ to the indicated cell potentials. Solid lines are fitted by simulation.

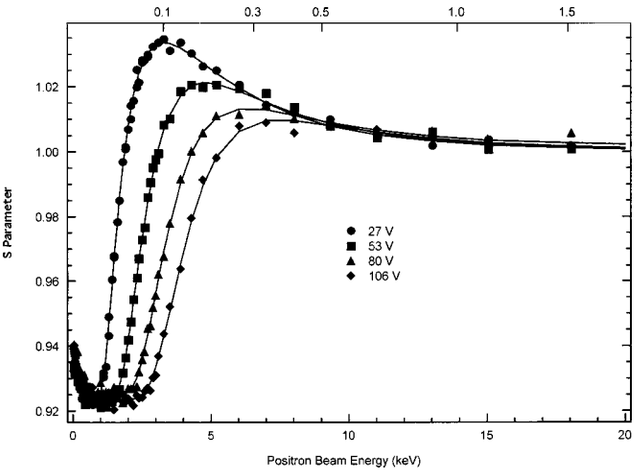


**Figure 2.** *S*-energy profiles of 15 min NaOH-treated aluminum foils after anodic oxidation at 2.5 mA/cm$^2$ to the indicated cell potentials. Solid lines are fitted by simulation.

Positron measurements were conducted in a vacuum system at $10^{-7}$ Torr. The positrons were emitted from a $^{22}$Na source; after passing through an energy monochromator they are implanted within the sample to an energy-dependent mean depth. At each beam energy, a Doppler-broadened gamma radiation spectrum was measured using a Ge detector mounted perpendicular to the beam direction; each spectrum consisted of about $10^6$ photon counts. *S* and *W* shape parameters of the annihilation photopeak at 511 keV (corresponding to the annihilation fraction with low and high momentum electrons) were calculated by the system software, to within an accuracy of 0.001. *S* and *W* are ratios of specific portions of the photopeak area to the total photopeak area: *S* refers to the central part of the photopeak near the maximum signal at 511 keV, and *W* to energies in the extremes of the photopeak, away from the maximum. Annihilation by valence and core electrons, respectively, contribute the portions of the photopeak measured by *S* and *W*. Because the contribution of valence electrons is enhanced near open-volume defects, relatively high *S* and low *W* values characterize positron annihilation in defective regions. The positron diffusion length for bulk aluminum was found to be 150 nm,[6] close to that reported for single-crystal aluminum samples.[2] Thus, the bulk condition approximates defect-free aluminum, consistent with the extensive annealing and large grain size of these foils. The *S* and *W* parameters were normalized to bulk aluminum values, obtained at beam energies approaching 20 keV. With this normalization, *S* and *W* values in Al greater and smaller than one, respectively, indicate the presence of open-volume defects.

PAS measurements of anodically oxidized as-received aluminum samples were carried out at Brookhaven National Laboratory, while those of anodically oxidized caustic-treated samples were done at Washington State University with similar low energy positron beam systems. For the same sample types, larger normalized *S* and smaller *W* parameters were obtained using the latter system, as a result of the improved energy resolution of its detector.[8] The comparison of *S* parameters obtained with the two systems is discussed in greater detail in the Results section.

## Results and Discussion

*S-energy profiles.*—Figures 1 and 2 show *S*-energy profiles for as-received and NaOH-treated foils, respectively. The data points are *S* parameters calculated from individual annihilation spectra measured at particular beam energies. The beam energy ($E_b$) on the top axis determines the mean implantation depth of positrons ($z_m$), according to the relation

$$z_m = \frac{40}{\rho} E_b^{1.6} \quad [1]$$

where $z_m$ is in nm, $E_b$ in keV, and $\rho$ is the density in g/cm$^3$.[2] The factor $40/\rho$ is 14.8 nm for aluminum, and 12.9 nm for anodic alumina; the top scale in Fig. 1 and 2 is calculated using the density of aluminum. The solid lines in the figures are the results of a simulation, to be discussed below. Further background material on *S*-energy profiles may be found in Ref. 7.

All samples have plateaus at low energy with low *S* values of 0.91-0.92. The range of energies occupied by these plateaus increases with anodizing voltage, suggesting that the plateaus correspond to layers which grow in thickness with increasing voltage. Further, these "plateau" *S* values are in agreement with prior measurements of aluminum oxide,[6-8,15] indicating that the plateaus represent the anodic oxide film. This assignment is supported by approximate agreement between the depth of the plateaus, as inferred from the top scales in Fig. 1 and 2, and the expected thickness/voltage ratio of anodic alumina, 1.3-1.4 V/nm.[16] For depths beyond the oxide plateau, there was a maximum on which, for most samples, *S* was larger than one. The maximum was followed at higher energy by a decay to a value of one corresponding to bulk aluminum.

Previously, *S* maxima at low energy were also found on foils with no anodizing treatment,[7,8,17] and were shown to be due to voids in the Al metal near the oxide/aluminum interface.[7,8] In Fig. 1 and 2, the absence of clear *S* maxima for the samples with thick films may have been due to "masking" of the defects by the oxide film, as opposed to the absence of interfacial defects. With increasing positron beam energy, not only the mean implantation depth but also the depth dispersion of implanted positrons increased. The depth distribution $P(z)$ is well approximated by the Makhov distribution[2]

$$P(z) = \frac{2z}{z_0^2} \exp[-(z/z_0)^2] \quad [2]$$

where $z_0 = 2/\sqrt{\pi} z_m$, and the Makhov parameter *m* is set to 2. According to Eq. 1, at $E_b = 5$ keV, the implanted positrons are spread over about 100 nm. Thus, a large fraction of positrons at this energy should be implanted inside the low *S* oxide and bulk aluminum phases, attenuating the contribution of any high *S* interfacial defects.

The masking effect of the anodic film was explored by removing the film in a chromic-phosphoric acid oxide stripping solution. Dissolution of the oxide layer in that solution was not followed by

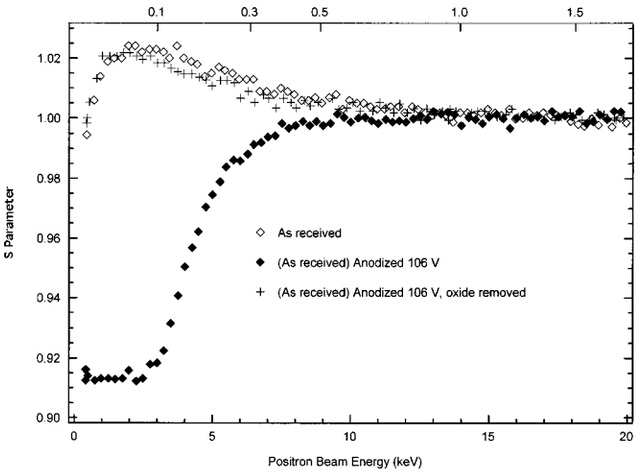


**Figure 3.** Comparison of *S*-energy profile of as-received aluminum foil to that of as-received foil anodically oxidized to 106 V, and that of as-received foil anodically oxidized to 106 V and then treated in an oxide stripping solution.

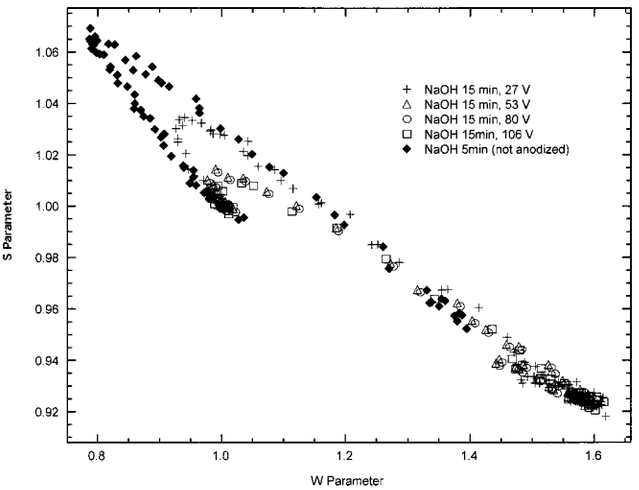


**Figure 4.** Plot of experimental *S* and *W* parameters for aluminum foils treated in NaOH for 15 min and then anodically oxidized to the indicated potentials. Also shown are *S*-*W* data of a foil treated in NaOH for 5 min but not anodically oxidized.

detectable mass loss due to aluminum corrosion,[6-8] because the chromic ions effectively passivated the metal. Hence, it was considered that any interfacial voids in the metal beneath the anodic film would be retained after stripping. Figure 3 shows *S*-energy profiles of an as-received foil before and after formation of a 106 V anodic film, and one measured after chemically stripping the film. No *S* maximum was present in the profile of the sample after anodizing, but stripping produced a *S* peak similar in shape to that of the as-received foil. When samples with no anodic film were treated in the stripping solution, no significant changes in the *S*-energy profiles were found. This is consistent with the previously observed association between the growth of *S* peaks and metal dissolution,[6-8] which did not occur at a measurable rate in the stripping bath. Thus, it is considered unlikely that the stripping treatment alone was responsible for the *S* peak. It is more probable that the *S* peak after stripping was due to interfacial defects in the metal beneath the oxide layer in the anodized sample, which were masked by the anodic oxide. This masking effect is considered further below, in the discussion of the simulations.

*S-W plot*.—Different types of open-volume defect are associated with particular *S* and *W* values. Hence, plots of the *S* parameter *vs.* the *W* parameter helped to identify the defects present in samples.[3,4] Background on the application of *S*-*W* plots to the aluminum samples is provided in Ref. 7. Figure 4 presents a plot of *S*-*vs.* *W* for the NaOH-treated foils, which includes all the *S* data from Fig. 2, but does not explicitly show the beam energy. For comparison, data are also presented for a foil which was treated by dissolution in NaOH for 5 min, but was not anodized. The *S*-*W* trace for this sample was analyzed previously.[7] It may be seen that this trace consists of two straight line segments, and that much of the data for the anodized foils fall along these lines. The lines connect clusters of points which define vertices at $(S,W) = (1.0,1.0)$, (0.92, 1.6), and (1.07, 0.78). There may be an additional cluster at (0.94, 1.45), which is difficult to resolve from the other high *W* vertex. The maximum *S* regions of the traces for anodized samples do not approach the high *S* vertex (defined by the foil with no anodic film), and show curvature as they bridge the two straight segments.

Vertices on *S*-*W* plots are interpreted as states such as phases or particular kinds of defects.[3,4,7] The vertices mentioned above with *S* values of 1.0, 1.07, 0.92, and 0.94 would represent aluminum metal, an open-volume defect at the metal/film interface, anodic alumina, and the oxide surface. For points along straight lines, annihilation occurs only in the two vertex states connected by the lines; curved regions of the trace suggest contributions from more than two states. In Fig. 4, data of the anodized samples appear to lie along the same oxide-defect and aluminum-defect line segments defined by the foil with no anodic film. This suggests that the same type of high *S* defect is found in both kinds of samples, in spite of the absence of high *S* data for the anodized foils. The curvature in the region bridging the straight lines is consistent with simultaneous contributions from the oxide, defect and aluminum states. The presence of high *S* defects in the anodized foils is not completely certain from Fig. 4 alone, because the defect-aluminum trace is not clearly established. On the other hand, such defects are also supported by the appearance of *S* maxima after oxide stripping (Fig. 3). A third source of evidence for high *S* defects, from simulations, is discussed below.

The interpretation of the *S* and *W* parameters of the interfacial defect was discussed in other papers.[7,8] The extreme values of these parameters indicate that the defect is a void of at least 1 nm radius. Larger defects cannot be distinguished using Doppler-broadening spectroscopy, because the *S* and *W* parameters saturate at about 1 nm, reaching values similar to those of infinite flat metal/vacuum interfaces. In fact, a similar high *S* value was measured on a clean aluminum surface.[17] Further, the high *S* and low *W* parameters relative to those of the oxide, and the agreement of *S* with measurements on clean aluminum, indicate that the void surface is oxide free. Therefore, the voids may lie along the metal/oxide interface, or within the metal beneath the film, but cannot be fully contained in the oxide. Because any exposure of a clean aluminum surface to water or oxygen would have resulted in a surface oxide film, the absence of oxide from the voids shows that they were formed internally by a solid-state process near the metal/film interface.

*Simulation of S-energy profiles*.—The *S*-energy profiles in Fig. 1 and 2 were simulated by solving the positron diffusion-annihilation equation. The simulations were carried out to determine important quantitative characteristics of the samples, such as the defect depth distribution and the oxide thickness. Simulations were accomplished by numerical integration, using the VEPFIT software application.[18] Further details on VEPFIT simulations of aluminum samples are found in Ref. 7. The samples were modeled as consisting of three layers, each having uniform properties: the anodic oxide film, an interfacial defect layer, and bulk aluminum. The simulation fit the parameters characterizing each layer, namely its thickness, characteristic *S* parameter and positron diffusion length. The fit defect layer *S* parameter (denoted $S_d$ below) corrects the measured *S* values for the effects of dispersion of implanted positrons (Eq. 2), and diffusion of positrons into adjacent layers. Because the oxide and

**Table I. Oxide layer parameters from simulations.**

| Anodizing voltage (V) | Oxide *S* parameter ($S_{ox}$) | Oxide thickness ($B_{ox}$, nm) | Voltage/ thickness |
|---|---|---|---|
| As-received | | | |
| 27 | 0.9072 | 28 | 1.02 |
| 53 | 0.9124 | 58 | 1.10 |
| 80 | 0.9129 | 104 | 1.30 |
| 106 | 0.9129 | 141 | 1.33 |
| NaOH treated | | | |
| 27 | 0.9213 | 27 | 1.00 |
| 53 | 0.9225 | 58 | 1.09 |
| 80 | 0.9240 | 102 | 1.28 |
| 106 | 0.9236 | 138 | 1.30 |

bulk aluminum have low *S* parameters compared to the defect layer, these effects tend to reduce the measured *S* below the true value for the defect layer. On the other hand, the parameter $S_d$ obtained by the simulation is determined only by the type of defects and their concentration in the defect layer. The positron diffusion length is the mean distance positrons diffuse before annihilating or trapping into defects, and is a decreasing function of the defect concentration.[2]

In the VEPFIT simulations, all model parameters were varied during fitting except the bulk aluminum diffusion length. This parameter was set to 150 nm, consistent with the diffusion length of single-crystal aluminum.[2] The initial estimates of the other model parameters were chosen to be physically realistic. Oxide and defect layer diffusion lengths were set to low values of about 1 nm, as done previously.[7] The oxide thickness was estimated according to the typical voltage/thickness ratio of 1.3 nm/V for anodic alumina films,[16] and the initial defect layer thickness was set to 15 nm for the NaOH-treated samples, and 150 nm for the as-received sample. These thicknesses are consistent with those of the samples before anodizing.[7] Since it was shown in Ref. 7 that more than 1 μm of metal dissolved in NaOH, the defect layer in the as-received sample was completely removed by dissolution; hence, the thinner defect layer in the treated sample contained new defects introduced by NaOH dissolution. Reference 7 provides a complete discussion of the effects of NaOH treatment on interfacial defects. Initial estimates of the layer *S* parameters were found by inspection of the data. The simulation fits are the solid lines in Fig. 1 and 2, which are seen to closely follow the data.

Table I shows the parameters of the oxide layer for all simulations. The oxide *S* parameter ($S_{ox}$) was 0.91 for the as-received samples and 0.92 for the NaOH-treated foils. These values are consistent with the low-energy plateaus in Fig. 1 and 2, and with prior measurements of anodic alumina films.[8,15] The oxide diffusion lengths (not shown) ranged from 1.0 to 2.0 nm for the NaOH treated foil and from 0.3 to 1.0 nm for the as-received foil. These values are smaller than the diffusion lengths previously measured for alumina films on intermetallic substrates.[19] However, the density of amorphous anodic films is significantly smaller compared to these oxides, suggesting that the anodic films should have a larger concentration of trapping sites and hence a smaller diffusion length. The fit film thickness ($B_{ox}$) increased with forming voltage, as expected. Table I shows that the ratio of the oxide thickness to forming voltage was consistently between 1.0 and 1.3, in reasonable agreement with the oxide thickness/voltage ratio of 1.2-1.4 expected for anodic alumina films.[16] The realistic oxide thickness lends support to the VEPFIT simulation results.

The thickness ($B_d$) and *S* parameter ($S_d$) of the defect layer, obtained by VEPFIT, are presented in Fig. 5 and 6. Figure 5 also shows the thickness of the layer of metal which was reacted to form the oxide ($B_{met}$). $B_{met}$ was calculated from the oxide thickness obtained by the simulation (Table I), along with the molar densities of aluminum in the oxide and in the metal. For the as-received sample, the increase of $B_{met}$ with oxide growth approximately parallelled the decrease of $B_d$. For example, at 70 V the consumption of metal (55 nm) was approximately equivalent to the reduction of the initial defect layer thickness (65 nm). This behavior can be explained by the consumption of the pre-existing interfacial defects during oxidation. For the NaOH-treated foil, $B_{met}$ exceeded the initial defect layer thickness of 25 nm at the potential of 40 V. At this point, the initial defect layer was completely consumed in the formation of oxide. However, a defect layer was present at higher voltages, in which the defects must have been formed by oxidation itself. Thus, the results in Fig. 5 for the NaOH-treated sample show that interfacial defects in the Al metal were created by anodic oxidation. The defect layer diffusion lengths obtained by the simulation were on average 1.1 nm for the as-received foil, and 5.0 nm for the NaOH-treated foil. There was no trend in either case with anodizing voltage. These small diffusion lengths relative to that of bulk aluminum (150 nm) are consistent with such layers found after dissolution processes.[7,8]

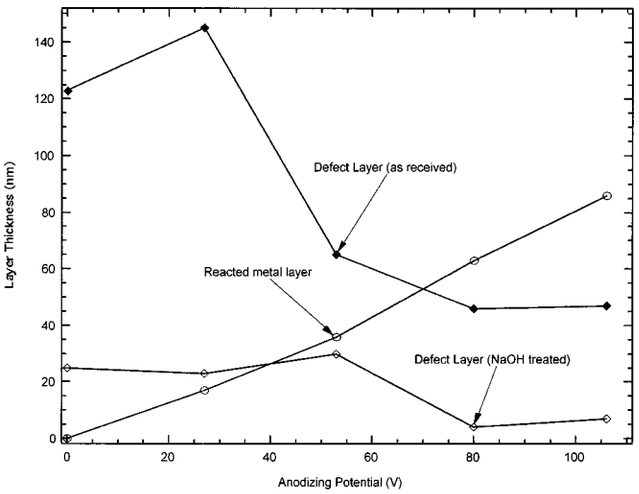


**Figure 5.** Model defect layer thickness *vs.* anodizing potential, for as received and NaOH treated foils. Also shown is the thickness of the metal layer converted to oxide, calculated from the model oxide layer thickness along with the molar densities of metal and oxide (Table I).

According to Fig. 6, $S_d$ of both sample types remained nearly the same during oxidation. For the as-received foil, $S_d$ was approximately constant at 1.02, while it was about 1.07 for the NaOH-

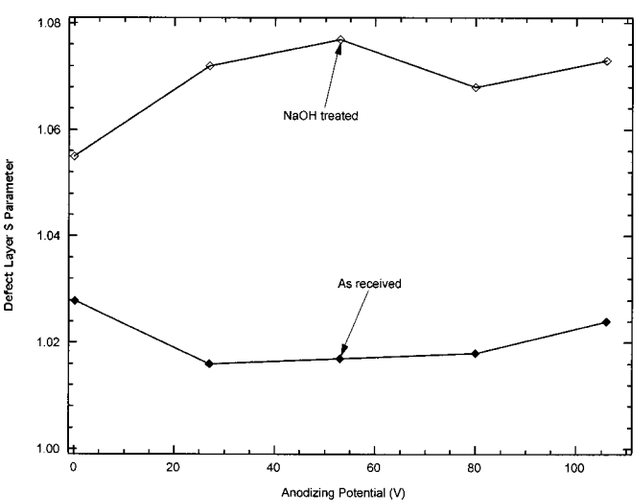


**Figure 6.** Model defect layer *S* parameter *vs.* anodizing potential, for as received and NaOH treated foils.

treated sample. As mentioned in the previous section, this latter value is similar to the surface *S* values for clean Al, suggesting that the voids are at least partially in the metal, and are larger than 1 nm in radius.[17] For the treated samples with thick anodic films, as discussed above, the *S*-energy profiles showed no pronounced peak. Nonetheless, the VEPFIT simulation reveals the presence of high *S* defects when corrections for annihilation in the low *S* oxide and aluminum layers are properly taken into account. Thus, the simulation provides additional evidence that the defects are voids of larger than 1 nm radius in the Al metal, corroborating that from the *S*-*W* plot and the oxide stripping experiment. Because data for the as-received and treated foils fell on the same *S*-*W* trace, the defects in the both kinds of sample were voids in the metal. [7] $S_d$ scales approximately with $f_D$, the void volume fraction in the defect layer[7]

$$S_d \simeq f_D S_D + (1 - f_D) S_B \qquad [3]$$

where $S_D$ is the intrinsic *S* value of voids ($\sim$1.07) and $S_B$ is unity, the *S* parameter of defect-free aluminum after normalization. Thus, the lower $S_d$ of the as-received foil was due to a smaller $f_D$. As mentioned above, the higher $S_d$ values of the NaOH-treated foils were partially due to the improved energy resolution of the detector used in those experiments. However, for samples with no anodic films, measurements with the same detector system have consistently shown a higher $S_d$ after 15 min NaOH treatment. For example, Ref. 6 reported a $S_d$ of 1.06 for the NaOH-treated foil *vs.* 1.03 for the as-received sample. The difference between these values is greater than the variation of $S_d$ with forming voltage in Fig. 6. Hence, Fig. 6 reveals a tendency for $S_d$ to remain constant at its initial value during oxidation, as the metal in the pre-existing defect layer is oxidized and new defects are formed. From Eq. 3, the constant $S_d$ during oxidation indicates that the volume fraction occupied by interfacial voids does not change, even as the void-containing layer is reacted to form oxide. Since nanometer-size voids should not be mobile, the constant $S_d$ might be explained by the ''regeneration'' of voids; that is, after pre-existing voids are incorporated into the film, new voids are created by oxidation at the same sites. This picture is consistent with the repeated formation of voids at certain ''defect'' sites at the metal/film interface. Such defects might be distinguished by segregated impurities, or topographic features such as microscopic asperities. Formation of voids at defects indicates that voids do not form at random locations on the surface, but that specific features of the site of oxidation are required.

Previously, Ono used high-resolution transmission electron microscopy to identify strings of voids in anodic alumina films, which were oriented perpendicular to the metal/film interface.[20,21] The images were interpreted by Macdonald to indicate that after a void was created at the metal/film interface, it became incorporated into the anodic film, and shortly thereafter another interfacial void was produced at the same interfacial site.[22] A similar process could be occurring in the present experiments, and would be consistent with the constancy of $S_d$.

## Conclusions

The formation of interfacial defects during anodic oxidation of aluminum was examined using Doppler-broadening positron annihilation spectroscopy. *S* and *W* shape parameters of the annihilation photopeak at 511 keV were determined, as a function of positron beam energy. Two types of annealed aluminum foil samples, as-received and NaOH-treated, were examined. Evidence was obtained from *S*-*W* plots, *S*-energy profile measurements after chemical dissolution of the anodic films, and simulations of *S*-energy profiles, that anodic oxidation resulted in the formation of open-volume defects at the metal/oxide interface. The high *S* and low *W* parameters of these defects indicated that they were voids of at least nanometer dimensions, lie wholly or partly within the Al metal, and have metallic surfaces free of oxide. For the NaOH-treated foil, evidence for interfacial voids continued to appear in measurements, after the metal within the pre-existing defect layer had been completely reacted to form oxide. This result showed that voids are formed during the process of oxidation. For both types of sample, simulations suggested that the area concentration of voids did not change appreciably during the growth of the anodic films. This could be explained by the repeated formation of voids at specific defect sites during oxide growth. Thus, void formation may be more complex than agglomeration of metal vacancies injected by aluminum atom ionization; certain specific features of the site of oxidation may also be required.

## Acknowledgments

Financial support for this work was provided by St. Jude Medical Corporation. Aluminum foils were donated by Nippon Chemi-Con. Research by PAK was performed under the auspices of the U.S. Department of Energy by University of California, Lawrence Livermore National Laboratory, with partial support from Basic Energy Research, Division of Materials Science.

*Iowa State University assisted in meeting the publication costs of this article.*

## References

1. H.-H. Strehblow, in *Corrosion Mechanisms in Theory and Practice*, 2nd ed., P. Marcus, Editor, p. 243, Marcel Dekker, New York (2002).
2. P. J. Schultz and K. G. Lynn, *Rev. Mod. Phys.*, **60**, 701 (1988).
3. P. Hautojärvi and C. Corbel, in *Positron Spectroscopy of Solids*, A. Dupasquier and A. P. Mills, Jr., Editors, p. 491, IOS Press, Amsterdam (1995).
4. A. van Veen, H. Schut, and P. E. Mijnarends, in *Positron Beams and Their Applications*, P. G. Coleman, Editor, p. 191, World Publishing Co., Singapore (2000).
5. P. Asoka-Kumar, K. G. Lynn, and D. O. Welch, *J. Appl. Phys.* **76**, 4935 (1994).
6. X. Wu, P. Asoka-Kumar, K. G. Lynn, and K. R. Hebert, *J. Electrochem. Soc.*, **141**, 3361 (1994).
7. K. R. Hebert, H. Wu, T. Gessmann, and K. G. Lynn, *J. Electrochem. Soc.*, **148**, B92 (2001).
8. H. Wu, K. R. Hebert, T. Gessmann, and K. G. Lynn, *J. Electrochem. Soc.*, **149**, B108 (2002).
9. J. E. Harris, *Acta Metall.* **26**, 1033 (1978).
10. C. Deacon, M. H. Loretto, R. E. Smallman, *Mater. Sci. Technol.*, **1**, 344 (1985).
11. Z. Ashitaka, G. E. Thompson, P. Skeldon, G. C. Wood, and K. Shimizu, *J. Electrochem. Soc.*, **146**, 1380 (1999).
12. X. Wu and K. R. Hebert, *J. Electrochem. Soc.*, **143**, 83 (1996).
13. C. E. Caicedo-Martinez, E. Koroleva, P. Skeldon, G. E. Thompson, G. Hoellrigl, P. Bailey, T. C. Q. Noakes, H. Habazaki, and K. Shimizu, *J. Electrochem. Soc.*, **149**, B139 (2002).
14. Z. Ashitaka, G. E. Thompson, P. Skeldon, G. C. Wood, H. Habazaki, and K. Shimizu, *J. Electrochem. Soc.*, **147**, 132 (2000).
15. T. van Hoecke, D. Segers, H. Schut, C. Dauwe, A. van Veen, B. van Waeyenberge, and L. Palffy, *Mater. Sci. Forum*, **255-257**, 724 (1997).
16. J. W. Diggle, T. C. Downie, and C. W. Goulding, *Chem. Rev. (Washington, D.C.)*, **69**, 365 (1969).
17. H. Huomo, E. Soininen, and A. Vehanen, *Appl. Phys. A: Solids Surf.*, **49**, 647 (1989).
18. A. van Veen, H. Schut, M. Clement, J. M. M. de Nijs, A. Kruseman, and M. R. Ijpma, *Appl. Surf. Sci.*, **85**, 216 (1995).
19. B. Somieski, L. D. Hulett, J. Xu, B. A. Pint, P. F. Tortorelli, B. Nielsen, P. Asoka-Kumar, R. Suzuki, and T. Ohdaira, *Phys. Rev. B*, **59**, 6675 (1999).
20. S. Ono, H. Ichonose, and N. Masuko, *J. Electrochem. Soc.*, **138**, 3705 (1991).
21. S. Ono, H. Ichonose, and N. Masuko, *J. Electrochem. Soc.*, **139**, L80 (1992).
22. D. D. Macdonald, *J. Electrochem. Soc.*, **140**, L27 (1993).